Chapter 4

# ZnO derived bioactive 1393 glass scaffold with enhanced biocompatibility and osteogenesis for neo-bone tissue regenerative application

## 4.1 INTRODUCTION

Cytocompatibility of a material is the cytological (cellular) compatibility or a state in which cells can grow, attach, differentiate and proliferate without being harmed while cultured onto that material. It may not be adequate describing a material cytocompatible using single type tissue or cell *in vitro*, since the implant-tissue interactions, immune response and damage repair functions in the body are so very complex (Kammula and Morris, 2001, Wang et al., 1997).

Metallic materials like titanium, steel, and alloys have been widely used as implant materials and contributed significantly to the global biomaterial market till date (Ivanova et al., 2014, Prasad et al., 2017). However, the biggest drawback of metallic implants is their material-tissue incompatibility which results in no biological fixation with the tissues and therefore accelerates the wear at the prosthetic region (Prasad et al., 2017). Even the so-called biocompatible titanium implants have provoked unwanted immune responses in metals on metals (MOM) joint prostheses, and total hip arthroplasty (THA), are a few of the examples of the drawbacks of metallic implants (Lehmann, 2017, Whittingham-Jones et al., 2008). Nevertheless, ceramic biomaterials, particularly bioactive glasses apart from *Autografts* and *Allograft (*gold standard for bone grafts) (Liu et al., 2013a, Bi et al., 2013), are so far the best synthetic grafting material because they are biologically compatible and can be converted to hydroxyapatites (the mineralogical component of bone

and teeth), and also can be tailored to the architecture of the physiological organs to mimic the natural tissues (Ali et al., 2018, Ali et al., 2020a, Ali et al., 2020b, Liu et al., 2013a).

However, zinc, the second most essential micronutrient of the body, is known for its involvement in fulfilling multiple functional activities in the human body (Prashanth et al., 2015). Its deficiency is characterized by stunted growth, delayed puberty, neuropsychological syndrome and osteoporosis like bone diseases (Baino et al., 2018, Park et al., 2018, Yamaguchi, 2012, Balasubramanian et al., 2015). Past research suggests that the zinc containing bioglass has enhanced bone metabolism and biocompatibility, controlled drug delivery, and prevented osteoclastic bone resorption (Goh et al., 2013, Bose et al., 2013). Still, the effects of Zn incorporated biomaterials are underexplored and needs further investigations.

## 4.2 MATERIALS AND METHODS

### 4.2.1 Sol gel derived BG and ZnBGs scaffolds and SBF preparation

The multicomponent 1393 glass based scaffolds were synthesized via wet-chemical sol-gel route by stepwise addition and hydrolysis of reagent grade precursors i.e., TEOS (assay 98%, Sigma-Aldrich, US), TEP (assay 99%, Sigma-Aldrich, US), $Ca(NO)_3.4H_2O$, $Mg(NO)_3$, $NaNO_3$, $KNO_3$ and $Zn(NO_3)_2$ (Assay >99%, Lobachemie, IN) followed by foam replication. The above mentioned precursors were added in required amount of 1(M) $HNO_3$ one after another maintaining at least 40 min of gap to allow complete hydrolysis of the precursors. 1-5 vol% PVA was added to the solution prior polyurethane foams of various dimensions ($2\times10\times10mm^3$, $10\times10\times10mm^3$ and $25\times10\times10mm^3$) were dipped into the sol during the process and were aged 48h for gelation. The hydrogel infiltrated foams after

aging for additional 2 days were dried at 80 ˚C for additional 48h. The foams were then heat treated at 1 ˚C/min up to 300 ˚C and hold for 4h to burn out the foams and binder and then sintered at 750-800 ˚C. However, the stoichiometric molar ratio of the ($H_2O$+$HNO_3$)/ (TEOS+TEP) was retained constant throughout the processes.

*Table 4.1: Percentage in chemical compositions (mol %) of BGs.*

| Chemical compositions | BG | Z1BG | Z2BG | Z3BG |
|---|---|---|---|---|
| SiO2 | 54.65 | 53.65 | 52.65 | 50.65 |
| CaO | 22 | 22 | 22 | 22 |
| Na2O | 6 | 6 | 6 | 6 |
| K2O | 7.9 | 7.9 | 7.9 | 7.9 |
| MgO | 7.7 | 7.7 | 7.7 | 7.7 |
| P2O5 | 1.75 | 1.75 | 1.75 | 1.75 |
| ZnO | 0 | 1 | 2 | 4 |

Simulated body fluid (SBF) to investigate *in vitro* bioactivity of the scaffolds was prepared as per the protocol of Tadashi Kokubo, and Hiroaki Takadama described elsewhere (,Oyane et al., 2003, Kokubo and Takadama, 2006, Ali et al., 2018). In brief, the required amount of reagent grade salts of sodium chloride, magnesium chloride hexahydrate (Merck, Germany), potassium chloride, dipotassium hydrogen orthophosphate trihydrate, calcium chloride, sodium bicarbonate and sodium sulfate (Lobachemie, India) and 1(M) HCl solution were added stepwise to the required amount of double-distilled water, buffered with tris-hydroxymethyl aminomethane until pH 7.4 achieved. The SBF solution was used for the *in vitro* bioactivity assessment of the scaffolds. *Table 4.2* corresponds to the ionic concentration of the SBF comparing human blood plasma.

*Table 4.2: Ionic concentrations in simulated body fluid and human blood plasma*

| Ions | $Na^+$ | $K^+$ | $Mg^{2+}$ | $Ca^{2+}$ | $Cl^-$ | $HCO_3^-$ | $HPO_4^-$ | $SO_4^-$ |
|---|---|---|---|---|---|---|---|---|
| SBF (mmol/L) | 142 | 5 | 1.5 | 2.5 | 147.8 | 4.2 | 1 | 0.5 |
| Human Blood Plasma (mmol/L) | 142 | 5 | 1.5 | 2.5 | 103 | 27 | 1 | 0.5 |

## 4.3 METHODS

### 4.3.1 Assessment of bioactivity

*The in vitro* bioactivity of the glass samples (powder/ scaffold construct) after soaking into the proportionate amount of SBF for specific days was assessed through X-ray Diffractogram (XRD), Fourier Transform IR spectroscopy (FTIR), Scanning Electron Microscopy (SEM), Energy Dispersive Spectroscopy (EDS) and pH behavior.

#### 4.3.1.1 pH

The pH of the SBF solution after soaking the glass samples for a pre-determined time period was recorded using a digital pH meter (Universal Bio microprocessor, India). The pH meter was calibrated each time with the standard buffered solution before measurements. The results were taken in triplicate (n=3) and represented as mean ± SD.

#### 4.3.1.2 XRD

The XRD analysis of the glass powder (finely ground scaffolds) was performed over the angular range (i.e., 2θ) 10 to 80˚ at a 3˚ $min^{-1}$ scan rate by using RIGAKU Miniflex II X-ray diffractometer equipped with graphite monochromatized Cu-$K_\alpha$ source and Ni filter operated at 40 kV tube voltage, and 20 mA current. The peaks were analyzed using standard ICDD (International Centre for diffraction Data) cards.

#### 4.3.1.3 FTIR

The functional groups responsible for certain characteristics in the scaffolds were identified by using BRUKER Tensor 27 Fourier Transform Infrared Spectrometer (FTIR, Germany) in transmittance mode within the frequency range of 4000- 400 $cm^{-1}$ taking 32 scans with a resolution of 4 $cm^{-1}$.

#### 4.3.1.4 SEM-EDS

The scaffold constructs were gold coated for 115 sec with a gold sputter and subjected to the smart SEM instrument, ZEISS EVO|18 (US) equipped with EDAX at 20 keV EHT for morphological study. The HA formation was assessed by examining the scanned micrographs of the scaffolds. The Ca/P ratio was estimated by quantifying the elemental atomic % over the scaffolds by EDX analysis.

### 4.3.2 Cell culture and *in vitro* assessment of cytocompatibility

#### 4.3.2.1 Cells and Cell Culture

Human osteosarcoma cell (U2OS) was purchased from American Type Culture Collection (ATCC, Manassas, USA), and the mouse cells NIH/3T3 cells from- NCCS, Pune, India. The cells were cultured in RPMI 1640 (Himedia, India) supplemented with 10% fetal bovine serum (Himedia, India), 100 U/ml penicillin, and 100 µg/ml streptomycin (Invitrogen, Carlsbad, CA), henceforth considered as a complete medium.

#### 4.3.2.2 Primary mouse bone marrow stromal cells (mBMSCs) isolation and culture

Primary mouse bone marrow derived stromal cells (mBMSCs) were isolated from the bone marrow of 8 weeks old wild type CD1 mice as described previously elsewhere(Hira et al., 2014b). In brief, the femur and tibia were dissected from mice, and bone marrow was flushed out with complete isolation media (CIM) containing RPMI-1640, supplemented

with 10% fetal bovine serum (Himedia, India), 100 U/mL penicillin and 100 µg/mL streptomycin (Invitrogen, Carlsbad, CA). Cells were washed with PBS, filtered (through 70 µm nylon mesh filter) and cultured in a 6 well cell culture plate in 5% $CO_2$ incubator at 37 °C. Non adherent cells were removed after 24h, passage 0 (p0) and subcultured in 6 well cell culture plate (p1). Cells were passaged every week using 0.25% trypsin/1 mM EDTA. BMSCs (p1) at 90% confluence were sub cultured at a 1:2 split ratio in complete culture medium consisting of Iscove modified Dulbecco medium (IMDM; GIBCO) supplemented with 10% FBS, 5 ng/mL basic fibroblast growth factor (βFGF), 100 U/ml penicillin, 100 µg/ml streptomycin (Invitrogen, Carlsbad, CA), and 12 µM L-glutamine (Invitrogen, Carlsbad, CA). BMSCs at 90% cell confluence were continued subcultured at 1:2 split ratio in CCM supplemented with βFGF (5 ng/mL) for several passages.

#### 4.3.2.3 Mouse blood cells isolation and culture

Mouse blood was collected from tail vein and the mononuclear cells (Lymphocytes and Monocytes) were isolated by gradient centrifugation using Ficoll-Hypaque. Isolated mononuclear cells were washed with RPMI-1640 supplemented with 5% FBS. The cells were re-suspended and collected by diluting with diluting fluid (10µl W.B.C) and cultured with complete medium before investigation.

#### 4.3.2.4 Cell viability, proliferation and cytotoxicity

As the cells become confluent, the scaffold constructs were readied by sterilizing with 70% ethanol and UV treatment. The scaffolds were then placed with the cell suspension containing $1\times10^5$ cells/well and cultured for 10 days with 5% $CO_2$ in a humidified atmosphere at 37˚C.The *in vitro* cellular viability of mBMSC, PBMC and NIH/3T3 cells,

after placing the scaffold constructs in the culture for an indicated time period, was assessed through XTT assay. However the cell proliferation study of U2OS and NIH/3T3 cells for 48h, 72h and 120h was investigated using CellTiter 96® Non-Radioactive Proliferation assay (MTT) kit from Promega. Further, the lytic activity of the bone marrow stromal cells (BMSC), white blood cells (Lymphocytes and Monocytes), cancer cells (U2OS), and normal embryonic fibroblast cells (NIH/3T3) was measured after 16h of incubation with the scaffold construct considering the cells being cultured alone as LDH control. LDH released in the culture supernatant was measured with 30 min coupled enzymatic assay. The absorbance for the viability, time dependent proliferation and cytotoxicity were measured at 475nm, 570nm and 490 nm respectively for percent specific calculation using the following formulae as described elsewhere(Hira et al., 2014b, Hira et al., 2014a).

$$\% \text{ Cell Viability} = \frac{\text{Experimental } OD_{475}}{\text{Control } OD_{475}} \times 100$$

$$\% \text{ Proliferation} = \frac{\text{Experimental } OD_{570} - \text{Blank}}{\text{Control } OD_{570} - \text{Blank}} \times 100$$

$$\% \text{ Cytotoxicity} = \frac{(\text{Experimental} - \text{Target Spontaneous})}{(\text{Target Maximum} - \text{Target Spontaneous})} \times 100$$

#### 4.3.2.5 Dual AO/EB Staining to Detect Apoptosis

Viable (live) and apoptotic (dead) cells were identified using Acridine Orange (AO) and Ethidium Bromide (EB) staining. To evaluate the apoptosis induced by the indicated compounds, different cells (U2OS, NIH/3T3 or mBMSC) were treated with 10µg/ml indicated materials for 48h, and were washed three times with PBS for 5 min. After fixing the cells with cold methanol for 20 min and another three PBS washes for 5 min were done

and permeabilization was done using Triton-× for 5 min and then washed again with PBS. In another set of experiments the mBMSC were cultured for 7 days with indicated scaffolds and subjected to similar process of preparation as stated above for dual AO/EB staining. The working solution of AO and EB mixture was prepared by means of adding1 µL of the AO/EB stock solution into a fresh Eppendorf tube containing 100 µL of phosphate-buffered saline (PBS) followed by mixing with 1:1 ratio fluorescent dye (100 µL) and cells (100 µL) and were left at room temperature for 15 min in the dark before analysis. Fluorescent images of the cells were obtained using fluorescence microscope Leica DMi8 (Germany) at 400× magnification.

#### 4.3.2.6 Evaluation of osteogenic differentiation capacity of the scaffolds on mouse Primary mouse bone marrow stromal cells (mBMSCs)

##### 4.3.2.6.1 ALP activity

To evaluate the alkaline phosphatase (ALP) activity in mBMSCs cells were grown with our derived scaffolds for 10 days and were subsequently harvested by trypsinization. Cells lysates were prepared with lysis solution (2% Triton ×-100 and 5mM $MgCl_2$) and the lysate was subjected to the alkaline phosphatase activity assay using Alkaline Phosphatase Diethanolamine activity Kit from Sigma as per manufacturer's protocol (Cat. No. AP0100; Sigma). Briefly, the colourless p-nitrophenyl phosphate (p-NPP) solution (0.67M) was prepared by addition of 247 mg of pPNPP into 1ml of ultrapure water followed by dilution of 0.15 mg/mL of both enzyme (ALP) and test solution in cold Reaction Buffer. Calculation of the ALP activity after 980µL and 960µL Reaction Buffer (1M Diethanolamine; pH 9.8, 0.5mM $MgCl_2$ )were taken in separate cuvettes (for Blank and test/enzyme control) followed by addition of 20µL 0.67M pNPP solution in each cuvette and 20µL of test

sample in test cuvette and 20µL of diluted ALP solution in enzyme control was done by the formula below. However the conversion of colorless pNPP into colored p-nitrophenol (yellow) in alkaline medium (pH = 9.8) was quantified (ALPase) using a colorimetric plate reader at 405nm.

$$\text{ALP activity} = \left(\frac{(\text{Abs}_{\text{test}} - \text{Abs}_{\text{blank}}) \times \text{df} \times \text{Vf}}{18.5\text{VE}}\right)_{\lambda=405\text{nm}} \text{ IU/L}$$

Where Df =dilution factor; Vf = volume of assay; VE = volume of test sample and 18.5 is the molar extinction coefficient at 405nm

#### 4.3.2.6.2 RNA isolation and reverse transcriptase polymerase chain reaction (RT-qPCR)

Primary mouse bone marrow stromal cells (mBMSCs) after grown with the scaffold constructs for 10 days and were trypsinized and harvested. Total RNA extraction was done using Total RNA Miniprep Purification Kit HiPurA™ (Himedia, IN) andwas carried out according to the manufacturer's protocol. Isolated RNAs were thenreversed transcribed to complementary DNA (cDNA) using HiScript One Step RT-PCR Kit. Briefly, the quantitative PCR study was performed in primer specific osteogenic genes osteopontin (OPN), osteocalcin (OCN) and glyceraldehyde-3-phosphate dehydrogenase (GAPDH) using Prima-96™ Thermal Cycler after denaturation (at 95°C for 1 min 45 s in 26 cycles of a three step cycle i.e. 95°C for 15 s, 57°C for 30 s, and 72°C for 1 min 55 s), and extension (at 72°C for 10 min). The transcribed product was visualized with 1%agarose gel electrophoresis and images of gel bands were analyzed with ImageJ software for quantification. The optical intensities were optimized with GAPDH.

*Table 4.3: Osteopontin (OPN), Osteocalcin (OCN) and Glyceraldehyde-3-phosphate dehydrogenase (GAPDH) primer for quantitative reverse transcriptase polymerase chain reaction (RT-qPCR) analysis*

| Genes | Sequence | Primer (Forward) | Primer (Reverse) |
|---|---|---|---|
| OPN | 5'→3' | CTTTCACTCCAATCGTCCCTAC | GCTCTCTTTGGAATGCTCAAGT |
| OCN | 5'→3' | GGGAGACAACAGGGAGGAAAC | CAGGCTTCCTGCCAGTACCT |
| GAPDH | 5'→3' | AGGAGTATATGCCCGACGTG | TCGTCCACATCCACACTGTT |

### 4.3.3 Mechanical and physical properties of the scaffolds

#### 4.3.3.1 Compression and bending strength of the porous scaffolds

Strengths of the scaffolds were measured in terms of compression ($\sigma_c$), flexure ($\sigma_f$) and their elastic modulii ($E_f$). Three point bend or flexural stress of the porous scaffolds with rectangular dimensions of 25×10×10mm$^3$ was measured in accordance with ASTM C1674-11 under a universal testing machine (UTM) H10KL (Tiniusolsen, US). Briefly, at least 5 sets of each scaffold were subjected to the 10KN uniaxial load maintaining the crosshead speed of 0.5mm/min. Similarly the glass scaffolds with 10×10×10mm$^3$ dimensions were tested for compression using standard protocol. Following formulas were used to calculate the mechanical properties of the scaffolds. Modulus of flexure ($E_f$) was calculated from the stress strain curve.

$$\text{Compressive stress, } \sigma_c = \frac{P}{A}$$

$$\text{Flexural stress, } \sigma_f = \frac{3PL}{2BD^2}$$

$$\text{Strain, } \varepsilon = \frac{6Dd}{L^2}$$

$$\text{Modulus of flexure, } E_f = \frac{L^3 m}{4BD^3}$$

Where P=load (Newton), A= surface area of load ($mm^2$), L =outer span length (mm), B= breadth of the scaffolds (mm), D= depth of the scaffolds (mm), d= deflection/ midspan (center of the beam) displacement (mm) and m= the gradient (i.e., slope) of the initial straight-line portion of the load deflection curve, (N/mm).

However, the porosities (AP) of the scaffolds were determined using solvent saturation method in methanol as follows

$$\%\ \text{Porosity} = \frac{w_s - w_d}{\rho V_a} \times 100$$

Where $w_s$is the saturated weight,$w_d$is the dry weight and $V_a$ is the apparent volume of the scaffolds; ρ is the density of methanol (0.792).

### 4.3.4 Statistical analysis

Statistical analysis of significance between pairs/columns was done by one way analysis of variance (ANOVA) followed by Tukey's post hoc test. Differences were considered significant for the 'p' value less than 0.05 (*) or 0.01(**) and 0.001(***). The results were presented as mean ± standard deviation (SD). All the experiments were performed in triplicates.

## 4.4 RESULTS

### 4.4.1 Structural, chemical, morphological and functional characterization for *in vitro* bioactivity

X-ray diffractogram depicts the fundamental structural differences between the SBF treated and sintered only samples. Fig 4.1A illustrates the evolution of distinctive characteristics peaks in the SBF treated scaffolds (above four) than that of the untreated (below four). The soaked in SBF for 15days glasses elucidated development of new peaks over the angular range 32˚, 45˚ and 56˚ for the entire sets of scaffolds. Predominant peaks representing particular phase(s) were observed with some minor alterations. Interestingly, the peak intensities were observed to be increased for the ZnBGs compared to the pure BG. Further, the XRD intensities corresponding ZnBGs, particularly Z4BG at 2θ= 45˚ and 56˚ increased manifold than the pure BG. Moreover, some exclusively explicit characteristic peaks for ZnBGs of both SBF treated and untreated samples were also observed.

Besides structural characterization, ZnBGs also differed from pure BG in pH behavior. The results demonstrate that the highest pH of 8.1 was observed in BG (Fig 4.1B) on day9. A continuous increase in pH uptoday7 was observed for the entire sets of scaffold, except Z4BG and then there was a decrease in pH thereafter.

SEM images (Fig 4.2) for the soaked in SBF scaffolds showed nonhomogeneous clusters or nodules or needle like flowery hydroxyapatites (HA) phases throughout the surfaces of the scaffolds. An estimation of quantitative Ca/P ratio (Fig 4.1C) acquired from EDS observations was found very close to the stoichiometric ratio of bone mineral (1.67).

*Table 4.4: Theoretical Vs EDS value in (Atomic)/ Mol%*

| Scaffold | Theoretical value | EDS obtained value |
|---|---|---|
| | Ca/P | Ca/P |
| BG | 6.28 | 1.76 |
| Z1BG | 6.28 | 1.69 |
| Z2BG | 6.28 | 1.97 |
| Z3BG | 6.28 | 1.67 |

FTIR spectral analysis from Fig 4.3 illustrates evolution of new resonances over the spectral range of 4000-400 $cm^{-1}$. Major modification in transmission spectra was observed within frequency range of 400-1000 $cm^{-1}$. The characteristics peaks representing particular functional groups were observed at 420 $cm^{-1}$, 460 $cm^{-1}$, 500 $cm^{-1}$, 570 $cm^{-1}$, 600 $cm^{-1}$, 690 $cm^{-1}$ and 1035 $cm^{-1}$. Some mild to moderate intense resonances were also observed within 1200-1700 $cm^{-1}$ and 2700-3700 $cm^{-1}$.

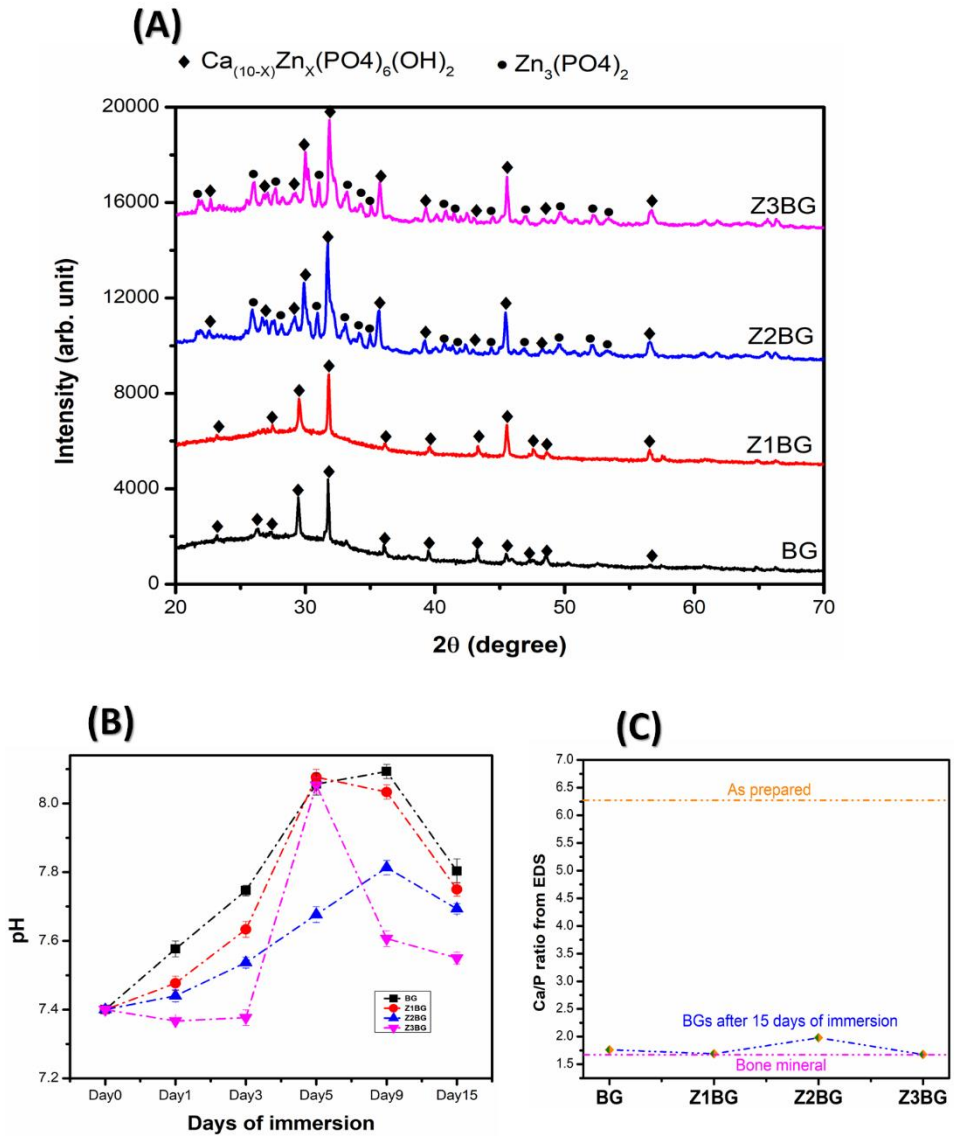


**Fig 4.1** X-Ray Diffractogram of 'soaked in SBF for 15days' samples showing crystalline hydroxyapatite (HA) formation over the angular range of 20 to 70° for the entire scaffold sets. **(B)** pH of the SBF solution as a function of materials (BGs) incubation time (days). (**C**) Elemental Ca/P ratio as an indication of surface reactivity to promote HA layer formation was estimated from atomic % of EDX analysis. The Ca/P ratio of prepared scaffolds (top), bone mineral (below) and conversion product formed on the glass based 1393 scaffolds (middle).

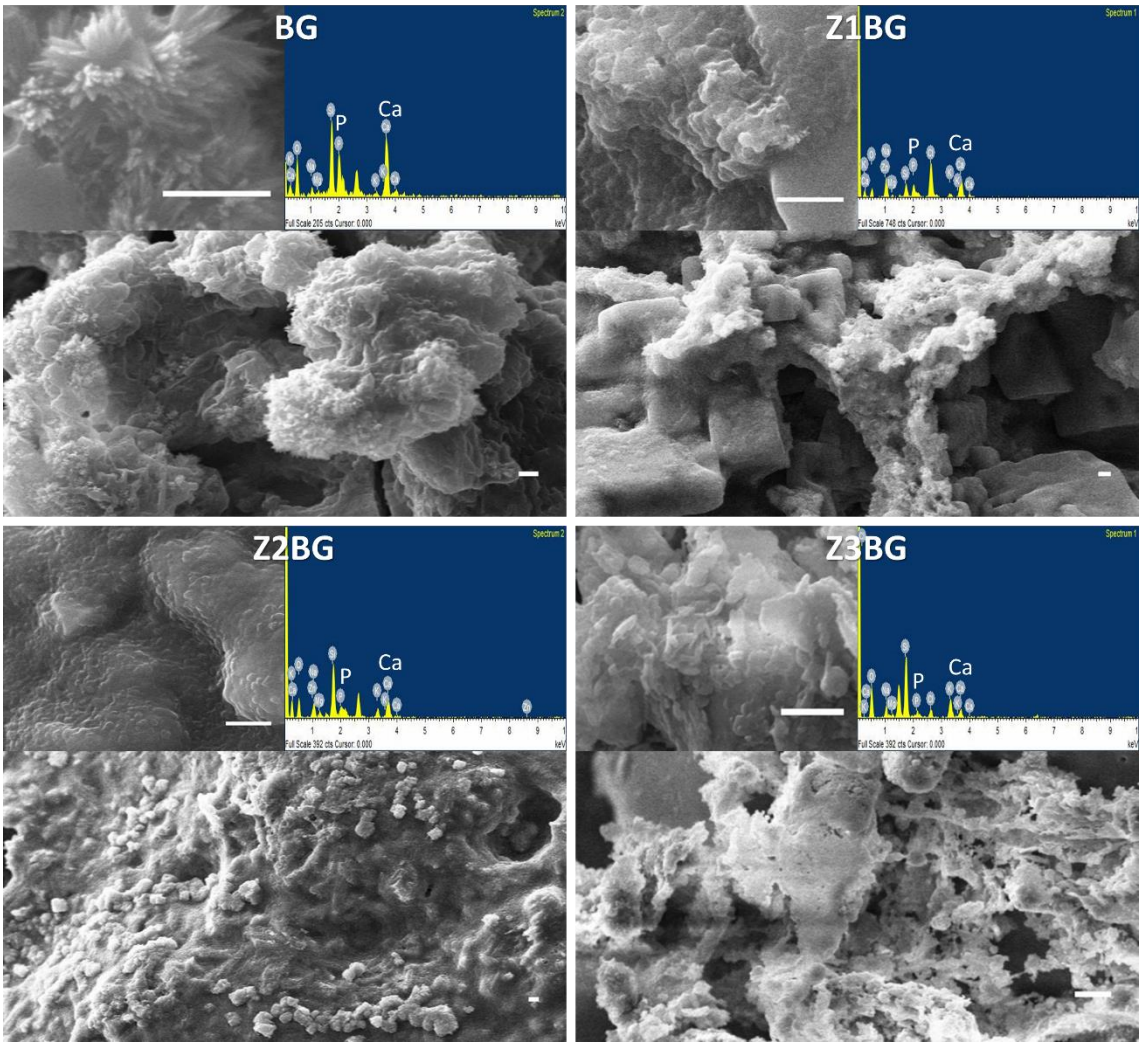


**Fig 4.2** SEM micrographs to evaluate bioactivity of the scaffolds showing formation of HA layer on the surface of the scaffold constructs. Energy Dispersive X-ray Spectroscopy (EDS) showing elemental presence of Ca and P (inside bar = 2µm).

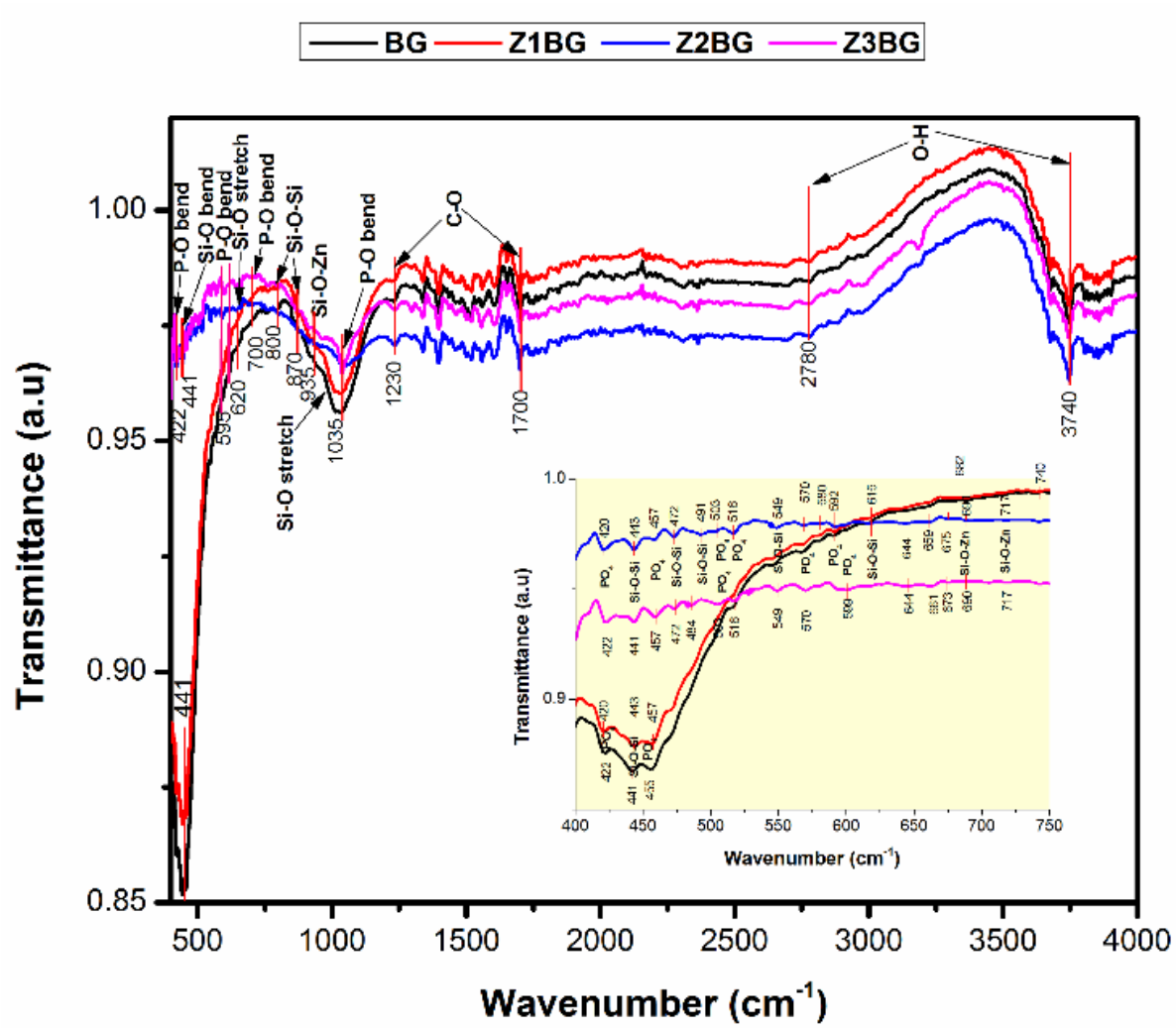


**Fig 4.3** FTIR spectroscopy showing characteristics functional group ($PO_4$) confirms HA layer formation for the soaked in samples.

### 4.4.2 The *in vitro* multi-cellular compatibility assessment on BG and ZnBGs

#### 4.4.2.1 Evaluation of Biocompatibility of BGs

Cytocompatibility of the cells in ZnBGs were compared with BGs. The *in vitro* cytocompatibility assessments were performed by using the stromal cells (BMSC), carcinogenic cells (U2OS), normal embryonic cells (NIH/3T3), and murine blood

mononuclear cells (monocyte and lymphocyte). All the cells after culturing into the bioactive glass-based scaffolds were assessed for *in vitro* biocompatibility of the scaffolds by means of viability, proliferation and cytotoxicity. The results (Fig 4.4A) demonstrate that the cells were viable in all of our derived scaffolds. Although the highest viability and proliferation and least toxicity was inconsistent for a particular scaffold. The results indicate that the highest % of viable BMSC cells at 50 µg/ml material concentration was 79.24 ± 0.66 in Z1BG. However, the viability of 82.78 ± 4.33 and 94.81 ± 2.67 of BMSCs were highest in BG, while the maximum viability of 86.56 ± 3.00 and 89.39 ± 5.67 at 10 µg/ml and 5 µg/ml were observed in Z3BG. Moreover, the least viability was always observed in Z2BG. Likewise, the viability of monocytes (Fig 4.4C) was insignificantly lowest at 85.47 ± 3.62 in Z2BG at 50 µg/ml but highest (94.27 ± 1.92) for lymphocytes (Fig 4.4B) at lower material concentration (2.5 µg/ml). In contrast, the BG showed the highest percentage of monocytes live cells (99.14 ±0.40) at 2.5 µg/ml (Fig 4.4C). Although the intra-groups (same material concentration) viability of BMSCs is not significantly different, yet the viability is statistically significant ($P<0.005$) in most cases while compared between groups (like 2.5 µg/ml vs. 50 µg/ml material concentration).

However, the live dead assay of NIH/3T3 cells incubated at 48h, 72h and 120h showed a different demonstration. The viable cells were found to be significantly ($P<0.005$) improved in ZnBGs than the pure BG while compared both in intra and inter groups. In fact, the viability was found to be increased with increase in Zn percentage in the glass system (Fig 4.5, A-C).

Nonetheless, the Z2BG showed the highest cell populations (92.18 ± 4.99 @ 48h, 89.94 ± 2.09 @ 72h, and 87.57 ±1.78 @ 120h) at 2.5 µg/ml materials conc., while the least cell

populations were observed in BG (76.68 ± 1.74 @ 48h, 68.63 ± 4.60 @ 72h, and 72.1 ± 3.56 @ 120h at the same materials concentration.

Similarly, the osteosarcoma (U2OS) cell proliferation assay demonstrates significantly improved ($P<0.05$) U2OS cellular proliferation in ZnBGs than the pure BG (Fig 4.6). Specifically, the Z1BG exhibited superior cellular proliferation against the BG at 2.5 µg/ml concentration. The Z2BG was, however, showed the least cellular proliferation (92.22 ± 0.28, 86.11 ± 0.83 and 71.93 ± 2.36) in almost entire osteosarcoma proliferation study (Fig 4.6, A-C).

The fluorescent microscopic images of mBMSC cells cultured into BGs at 10 µg/ml conc. for 24h and stained with AO/EB indicate the viable (live cells; green in color with an undisturbed membrane), early apoptotic cells (with bright green nuclei due to chromatin condensation), and the late apoptotic cells (with fluoresced orange/red nuclei) (Fig 4.6D).

Cytotoxicity (Fig 4.7, A-E) of the cells (U2OS, BMSC, NIH/3T3, monocytes and lymphocytes) after 16h co-culture with the scaffolds constructs were measured as LDH (lactate dehydrogenase) release at 490 nm. Irrespective of material concentrations, the lysis activity of cells was found maximum in BG compared to ZnBGs. Although there were no significant differences in cell lysis except a few, the lysis due to toxicity of materials was found lesser in ZnBGs than the pure one. However, the least U2OS cells lysis (Fig 4.7A) was observed in Z1BG (2.49 ± 0.71, 3.90 ± 0.51, 4.58 ± 1.091, 5.22 ± 1.22 and 8.62 ± 1.28 % for 2.5 to 50 µg/ml materials conc.) than the other BGs. Unlike U2OS the minimal cell lysis of embryonic cells was observed in Z2BG (i.e., 3.56 ± 2.27, 4.95 ± 3.65, 8.37 ± 0.20, 9.83 ± 1.1 and 12.48 ± 0.30 % @ 2.5-50 µg/ml materials conc.) (Fig 4.7C). It is worth noting that the least lymphocytic cell lysis of 2.60 ± 0.88 % was observed in Z2BG at 2.5 µg/ml (Fig 4.7D).

Also, the results demonstrate that Z1BG (also Z3BG) was found to be least toxic to the mBMSCs at 50, 10 and 5 µg/ml conc. (Fig 4.7B). However, the Z2BG was again found least toxic to the monocytic cells at 2.5 µg/ml concentration.

The *in vitro* apoptotic assay of stromal cells after culture with scaffolds for 10 days were assessed using AO/EB staining (Fig 4.8C). Results demonstrate the apoptotic cells with red nuclei (late apoptotic) or bright nuclei with chromatin condensation (early apoptotic) was higher for BG and Z1BG and least in Z2BG/Z3BG. The phase contrast microscopic images (400× magnification) of cells constructs showed BMSCs populations on day0 (Fig 4.8A) and survival, growth, differentiation and attachments on day10 (Fig 4.8B) over the scaffolds. All these microscopic images illustrate Z3BG/Z2BG are less apoptotic and better viable to the cells. The phase contrast microscopic images of BMSCs, NIH/3T3 and U2OS (Fig 4.9) after culture for certain periods corroborate the better survival, growth and cellular attachments in either of Z2BG or Z3BG.

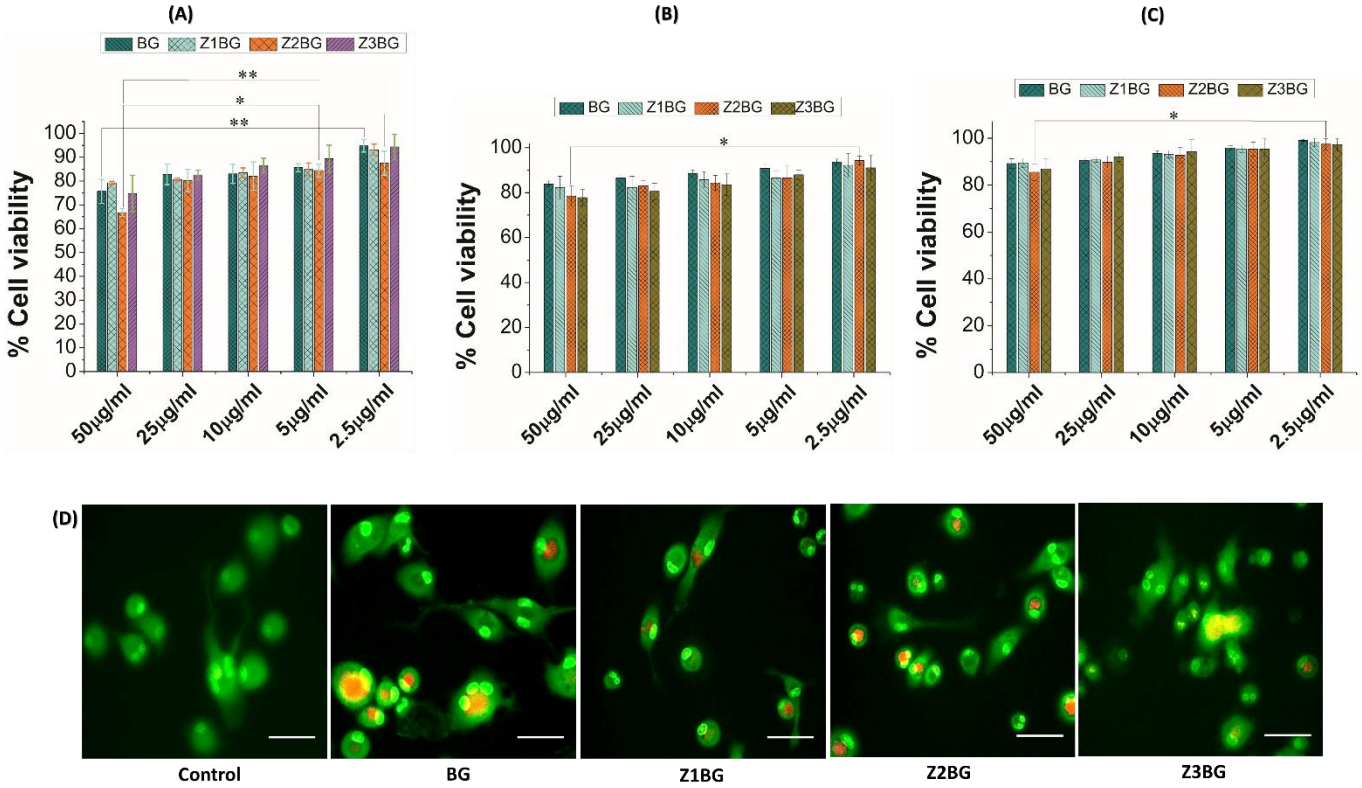


**Fig 4.4** Cellular viability of murine bone marrow stromal cells (**A**) and blood mononuclear cells (**B**&**C**-Lymphocytes & Monocytes). (**D**) Fluoresced images of AO/EB stained cells sowing viable (green), early apoptotic cells (bright green nuclei with chromatin condensation) and late apoptotic (orange/red) stromal cells after 24h culture in scaffolds (inside bar = 10µm).

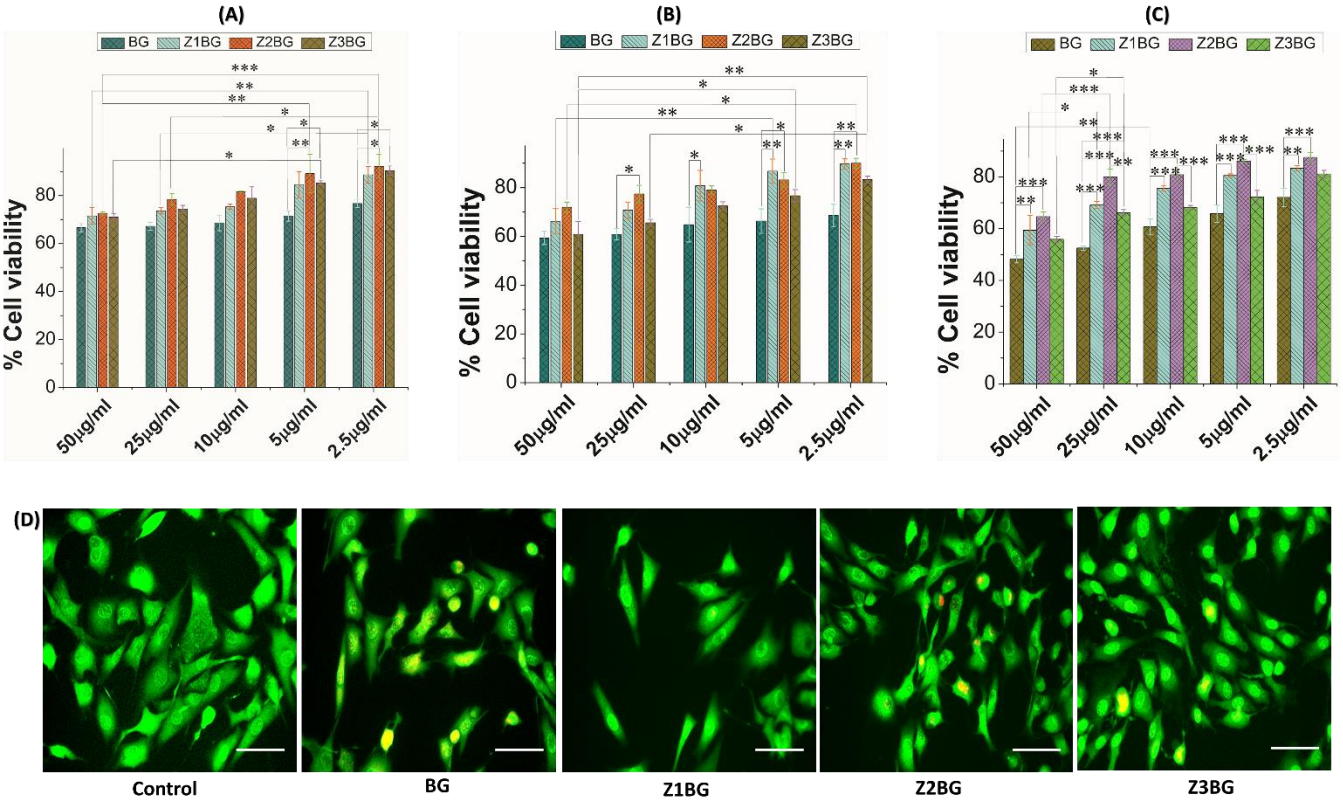


**Fig 4.5** Time dependent cellular viability of normal cells NIH/3T3 for (**A**) 48h, (**B**) 72h and (**C**) 120h. The results showing ZnBGs were cytologically more compatible as the normal mouse embryonic cells survived more in ZnBGs compared to BG (inside bar = 10µm).

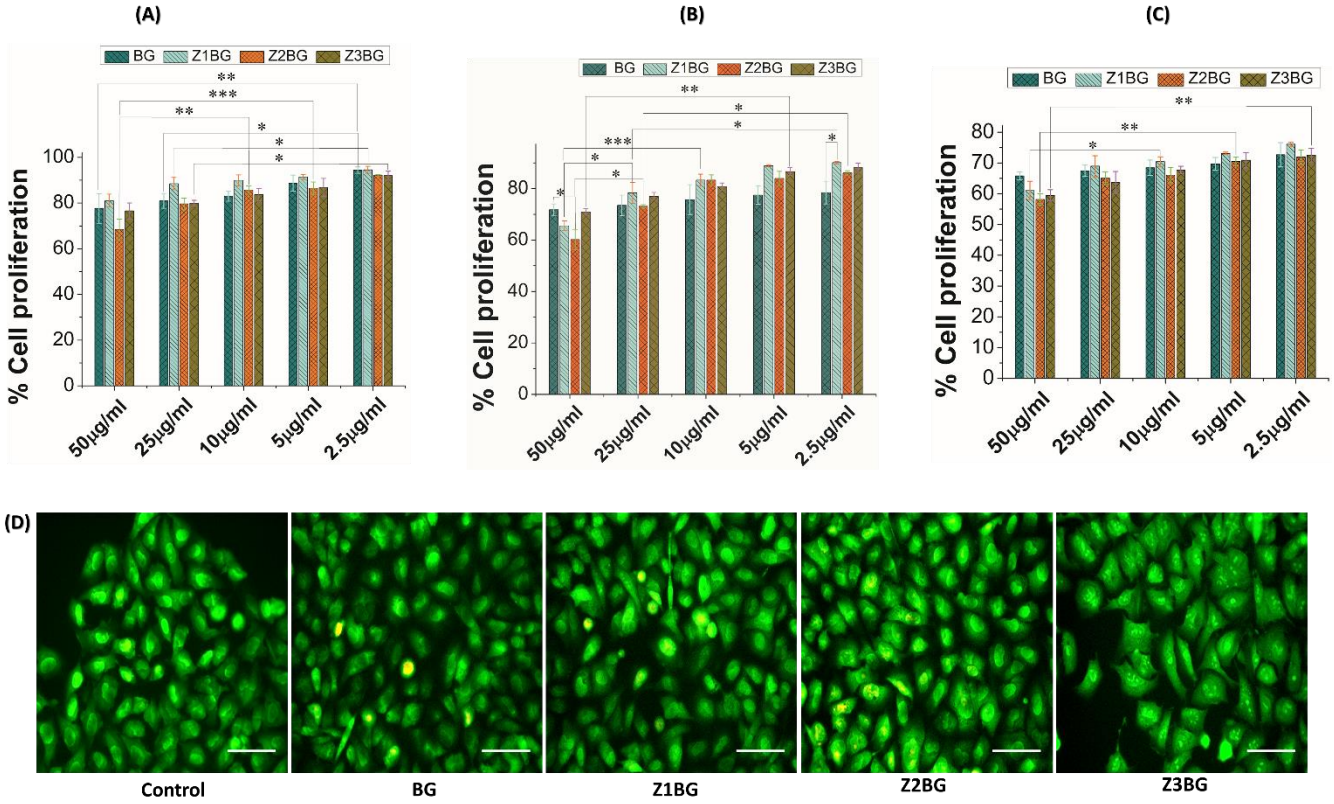


**Fig 4.6** Bar diagram represents % cell proliferation of U2OS cells in a time dependent ((**A**) 48h, (**B**) 72h and (**C**) 120h) manner by using MTT assay. Microscopic images show viable (green) and apoptotic (orange) cells stained withAcridine Orange (AO) &Propidium Iodide (PI). One way ANOVA followed by Tukey's post mean comparison for statistical significance analysis considered significant (*) for p value <.05 and highly significant (**) for <.01 and p<.001 (n=3) (inside bar = 10µm).

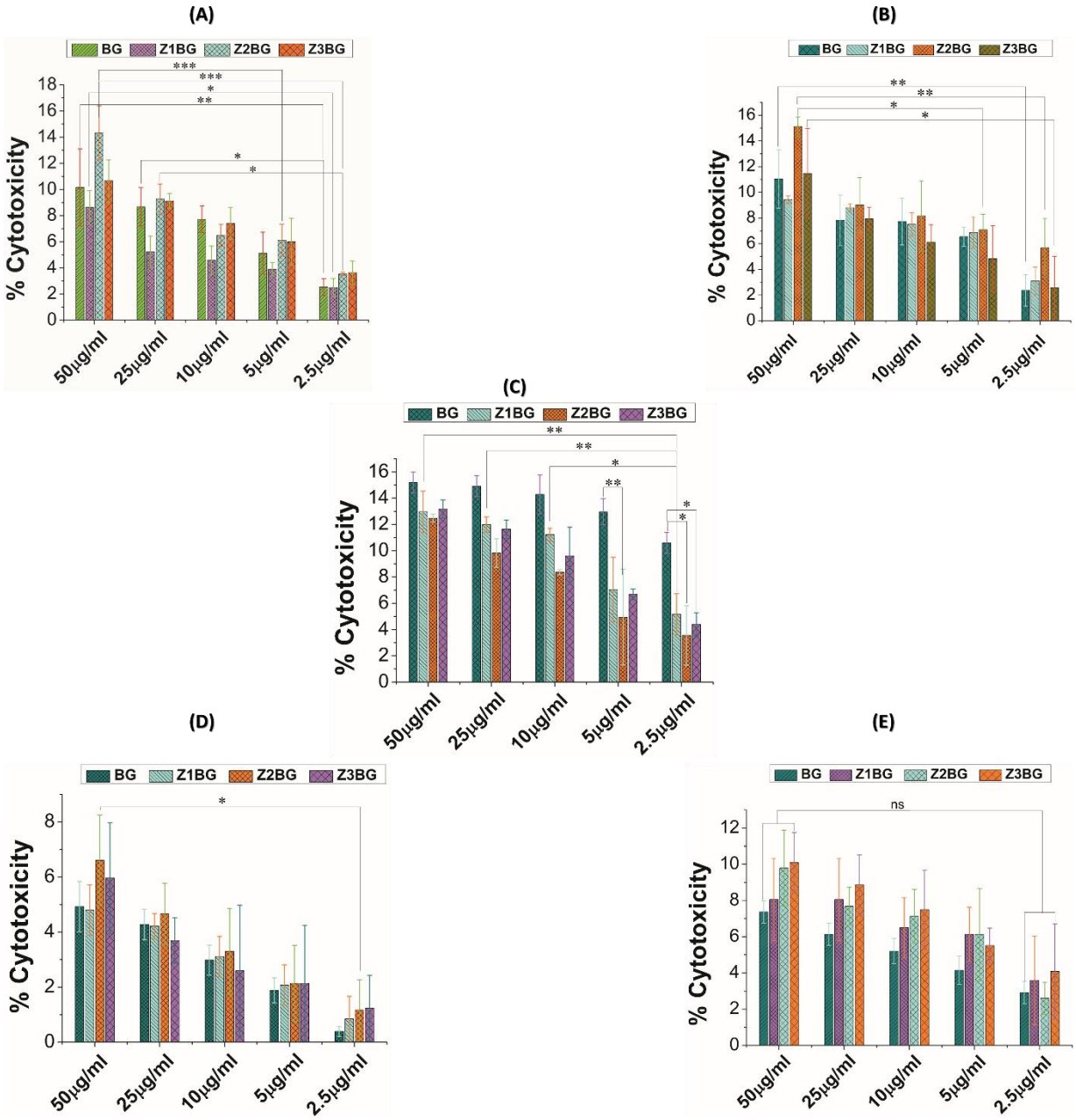


**Fig 4.7** Cytotoxic effect of BGs on **A**-U2OS, **B**-BMSC, **C**-NIH3T3, **D**-Monocyte and **E**-Lymphocyte cells as a measure of LDH release after 24h of culture on scaffolds. The statistical analysis (ANOVA) showing ZnBGs caused less cell lysis in comparison of BG in most cases.

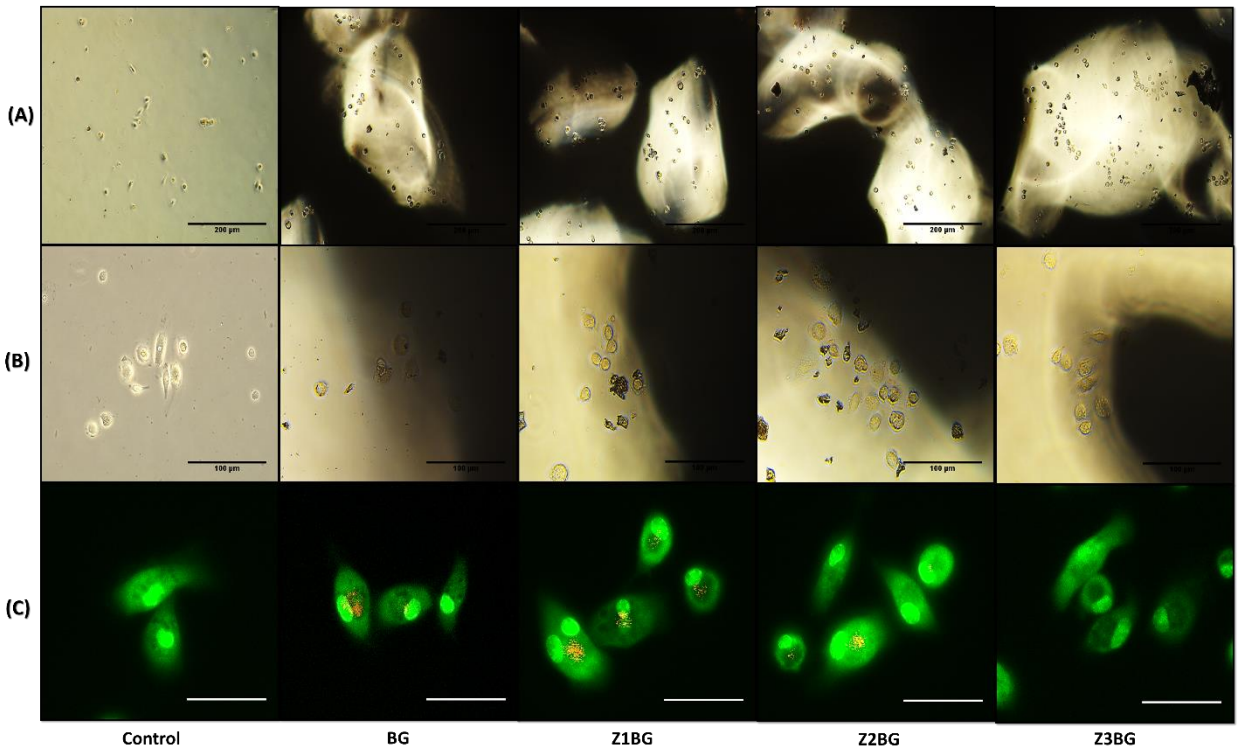


**Fig 4.8** *In vitro* effect of BMSCs upon glass scaffold implantation. Cell survivability of the stromal cells implanted of BGs was observed under phase contrast microscopy on day0 (**A**) and day10 (**B**). Fluoresced images (AO&PI) (**C**) show viable stromal cells on day10 [inside bars = 100µm (A), 200 µm (B), and 10µm (C)].

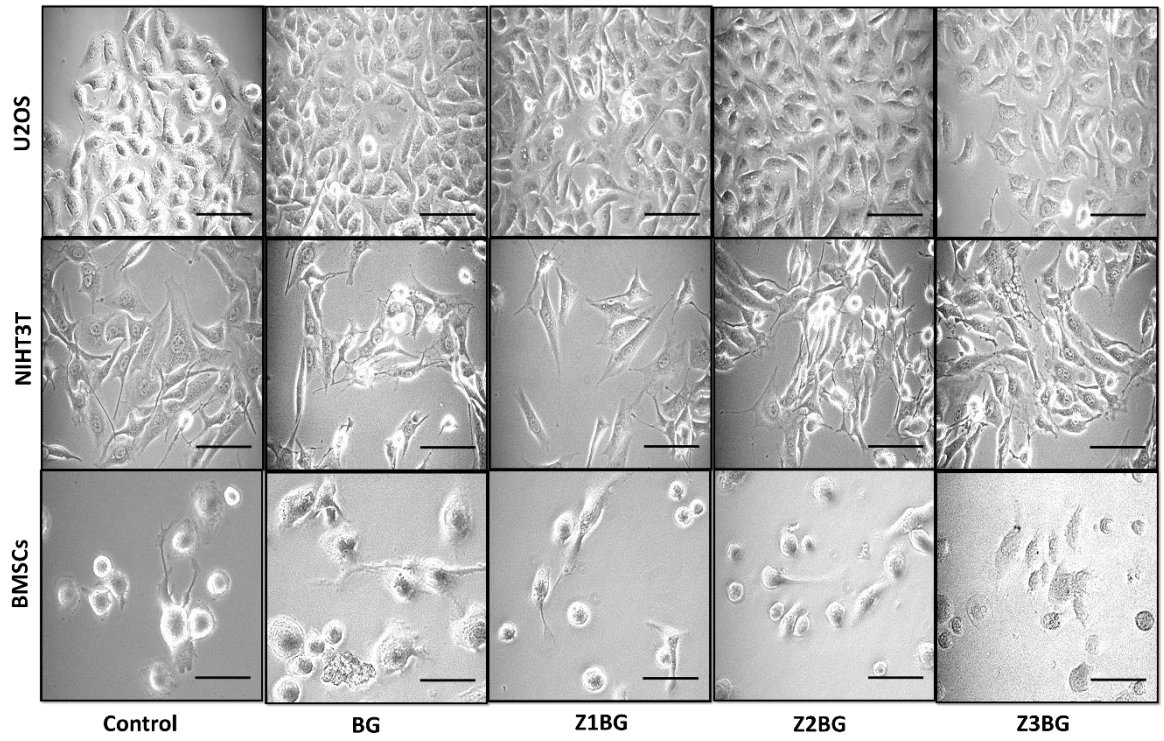


**Fig 4.9** Phase contrast microscopic images of viable cells (U2OS, NIH/3T3 and BMSCs) after grown onto glass derived scaffolds (BG, Z1BG, Z2BG and Z3BG) for 48h (inside bar = 10μm).

### 4.4.3 Osteogenic differentiation of BMSCs on BGs

#### 4.4.3.1 ALP activity

The alkaline phosphatase (ALP) is considered to be one of the best early osteogenic differentiation markers for bone formation. In this investigation, the enzymatic reaction kinetics catalyzed with alkaline reaction buffer (pH 9.8) of dimethanolamine and $MgCl_2$ was detected by converting the chromogenic pNPP substrate into yellowish water soluble pNP at 405 nm (Sun et al., 2018). The increase in ALP activity in osteogenesis is correlated with the initiation of bone mineralization by means of $Ca^{2+}$ uptake, and thus active bone formation.

However, it is worth mentioning that the detection of bone mineralization (by Alizarin red, etc.) was not performed here and will be included in our future studies. Herein, the results indicate that the increasing ALP activity was observed with the increase in zinc percentage in the parent glass (1393 bioactive glass) system. The highest ALP activity was found to be 10.72 ± 1.69 IU/L in Z4BG and the least ALP activity of 0.65 ± 0.56 IU/L was observed in BG. An insignificantly higher ALPase of BG over control was also observed at the same time. Furthermore, the ALP activity of Z1BG and Z2BG was 1.30 ± 0.56 and 4.20 ± 0.73 respectively.

### 4.4.3.2 Quantitative assessment of osteogenic gene expression by RT-qPCR

The expression of primer specific mid to later stage osteogenic differentiation marker genes OPN and OCN was assessed through semi-quantitative RT-PCR analysis by normalizing with GAPDH (housekeeping gene) values using NIH ImageJ software of electrophoretically visualized DNAs band intensities. The agarose gel electrophorectic images of OCN, OPN and GAPDH (Fig 4.10B) representing their own band intensities were measured and normalized with GAPDH for the quantitative analysis (Fig 4.10, C & D). The osteoblast specified OPN and OCN gene expression was up regulated (Fig 4.10) upon exposure the BMSCs to the derived scaffolds. However the upregulation in response to the stimulants was better in ZnBGs compared to BG. This present investigation showed a significantly higher ($p<0.005$)OPN and OCN gene expression in ZnBGs compared to BG. Likewise early osteogenic differentiation marker i.e. ALP, the increase in gene expression was continuous with the increase in zinc substitution in the parent 1393 glass scaffold (BG).

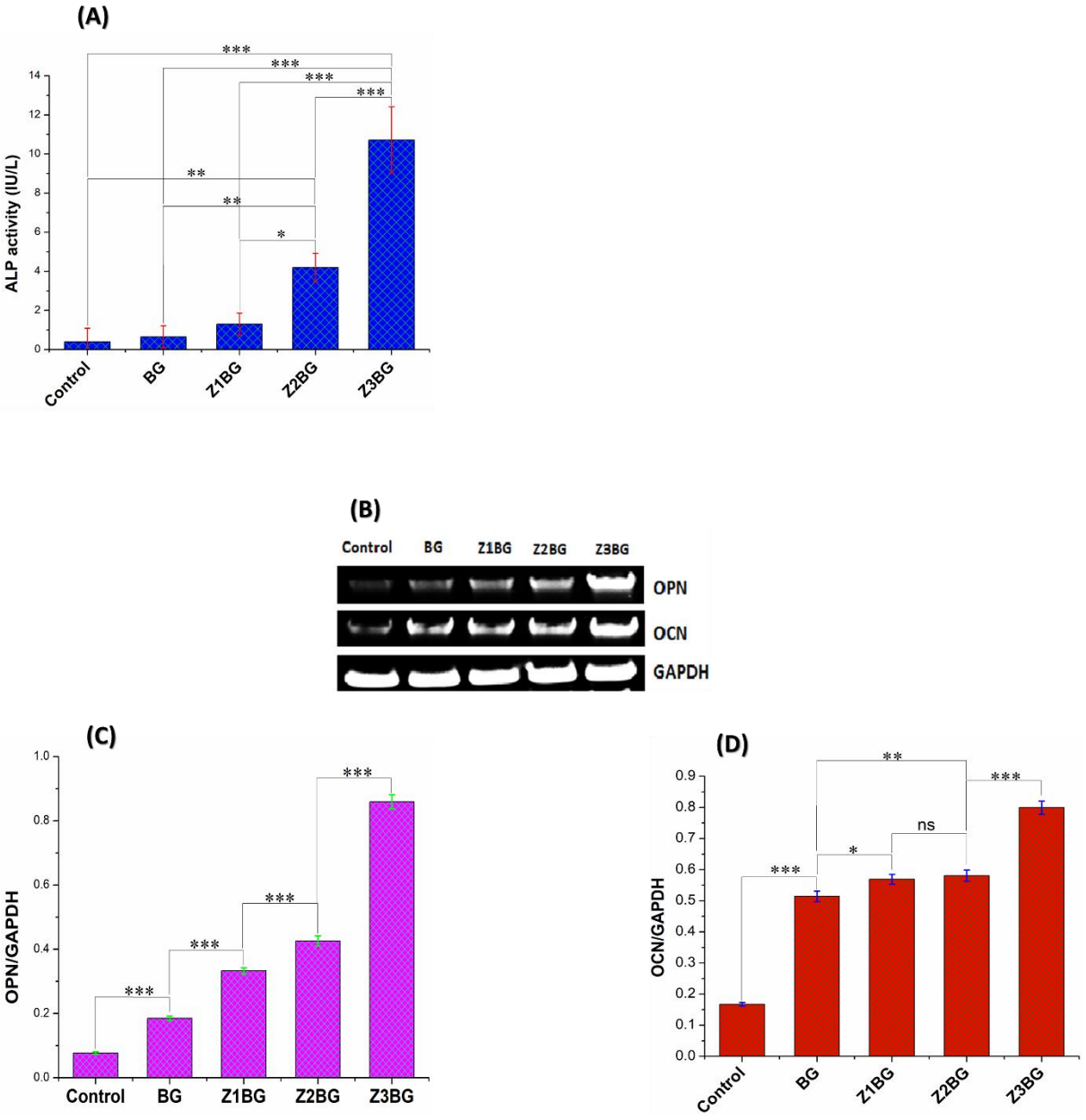


**Fig 4.10** Effect of osteogenic markers on inducing osteoblastic phenotype including ALP (**A**), OPN (**C**) and OCN (**D**). Agarose gel electrophoretically visualized images (**B**) showing DNAs band intensities of osteogic genes OPN, OCN and GAPDH. The band intensities were found increasing with increase in zinc percentage in BGs. Statistical analysis (ANOVA) of the early osteogenic differentiation marker (ALP) and mid to late osteogenic differentiation marker (OPN and OCN) induced osteoblastic phenotype on BMSCs appeared significantly highest in Z3BG and least in BG. Values were considered statistically significant (*) for p value <.05 and highly significant (**) for <.01 and p<.001 (n=3).

### 4.4.4 Mechanical performances of the scaffolds

In this study we have successfully synthesized the zinc based 1393 glass based scaffold with interconnected porosity (AP) >50 % through sol gel route. The mean compressive and flexural strengths appeared in this investigations were 7.2-12.7 MPa and 0.66-1.81 MPa.

However, the results demonstrates that the mean (n=5) compressive ($E_c$) and flexural ($E_f$) properties of BG, Z1BG, Z2BG and Z3BG were 7.2 ± 1.8 MPa, 7.9 ± 2.4 MPa, 6.6 ± 4.9 MPa and 12.7 ± 3.7 MPa and 0.66± 0.32MPa, 0.77 ± 0.27MPa, 1.2 ± 0.45 MPa and 1.81 ± 0.65MPa respectively (Fig 4.12). Further, the lowest and highest flexural value were observed to be 0.27Mpa (not shown) and 2.8MPa for BG and Z3BG respectively.

Moreover, the bending modulus (Fig 4.11) derived from stress-strain curves were found to be 246 MPa, 426 MPa, 408 MPa, 351 MPa for BG, Z1BG, Z2BG, and Z3BG respectively.

## 4.5 DISCUSSIONS

### 4.5.1 The *in vitro* bioactivity: structural and physico-chemical evaluation

Structural modifications in the scaffolds were analyzed through X-ray diffractogram for the evaluation of *in vitro* bioactivity. XRD spectra of the soaked in SBF samples depicting formation of several moderate to mild intense crystalline peaks were studied. Results demonstrate the formation of crystalline hydroxycarbonated-apatites (HCA) [PDF # 74-0565](Gergely et al., 2010).for the entire scaffold sets. The major peaks corresponding to HAs were primarily observed at the diffraction angle 32˚, 45˚ and 56˚. Interestingly, the increases in zinc percentage in BGs caused to have increase in HCA formation as the peak intensities were found increasing in ZnBGs (Fig 4.1 A) (Fernandes et al., 2018, Fiume et al.,

2018). The increase in peak intensities (Fig 4.1 A) of the soaked in SBF for 15d ZnBGs samples were attributed to the formation of zinc apatite ($Ca_{10-x}Zn_x(PO_4)_6(OH)_2$ (Miyaji et al., 2005, Qian et al., 2008). Besides, the increasing peak heights as Zn percentage in BGs increases, a gradual broadening of peaks at the base was also observed. The broadening of the peaks was, however, could be due to the fact that Zn has the tendency to lessen the crystallinity in hydroxyapatites(Miyaji et al., 2005). Moreover, several other mild to moderate peaks were also observed for the development of $Zn_3(PO_4)_2$ crystals over the ZnBGs. The presence of broad hump in XRD spectra for the SBF treated scaffolds can be argued due to the existence of glassy matrix phase in the scaffolds (Ali et al., 2018). Besides structural characterization, chemical evaluation (pH) for bioactivity assessment was also favored the formation of apatites. Bioactive glass or scaffolds undergone surface modifications through several chemical reactions (Islam et al., 2017b, Islam et al., 2017a, Vyas et al., 2016). The abrupt increase in pH (Fig 4.1 B) was due to the rapid exchange of surface cations (i.e. $Ca2^+$, $Na^+$, $Zn^{2+}$, $Mg^{2+}$, and $K^+$) with $H^+$ ions from the SBF solution resulting in increased the basicity of the solution. However the increase in pH is favorable for HCA formation by the fact that higher pH led to attack on the silica network causing network dissolution and subsequent silanol (SiOH) formation. The surface reactivity was then decreased by polycondensation of silanols and subsequent silica rich amorphous HA layer formation by means of adsorption of $Ca^{2+}$, ${PO_4}^{3-}$and ${CO_3}^{2--}$ ions glass surface (Islam et al., 2017a, Asokan and Cho, 2002, Ali et al., 2018, Ershad et al., 2017, Ershad et al., 2018, Yadav et al., 2017, Yadav et al.). The formation of silica rich amorphous HA layer and their gradual conversion to crystalline HCA cause to have cut the connectivity between surface cations and solutions resulting in decrease of pH after 7d.

Morphological study (Fig 4.2) also revealed the growth of HA nodules in the form of agglomerated needles (on BG) or nano-rods (BG) or randomly dispersed clusters (on ZnBGs) on the surface of scaffold constructs. Elemental quantification from EDS also suggests the presence of Ca and P ions on the scaffold surfaces (*Table 4.4*). The stoichiometric Ca/P ratio in 45S5 glass composition is 5, while in ours the ratio is~6. As per the Hench and other researchers' claim the materials with lower Ca/P ratio would not bind to bone and, thus will not be considered bioactive (Bang et al., 2008, Hench and Paschall, 1973). However, in this investigation the elemental EDS quantification confirmed the Ca/P (in BG) ratio and Ca+Zn/P ratio (in ZnBGs) (Fig 4.1 C) were also found within the anticipated range.

FTIR spectra corresponding SBF treated samples (Fig 4.3) demonstrate that the alteration in resonances at frequency (ν) 420, 460, 500, 570 and 600 $cm^{-1}$ were associated with bending vibrations of P-O bond (Rezaei et al., 2014, Bonartsev et al., 2017, Ulian et al., 2013). The modification in frequency at 1035 $cm^{-1}$ was attributed to the symmetric $PO_4$ stretching. Further, the resonances within the frequency range 1200-1700 and 2800-3600 $cm^{-1}$ were due to the vibrational stretching of C-O and O-H groups. Presence of P-O, C-O and O-H and Si-O-Zn functional groups in the spectral resonances was the indication for the growth of HCA [$Ca_{10-x}Zn_x(PO_4)_{6-y}(CO_3)_y(OH)_2$] like layers over the samples (Raevskaya et al., 2014, Ali et al., 2014).

### 4.5.2 The *in vitro* cytocompatibility: cell proliferation, survivability and growth and cytotoxicity of mBMSCs, U2OS and PBMC over BGs.

Dose (material concentration) *vs.* cell survivability of mBMSCs after 24h culture over scaffolds demonstrates insignificant cell lysis at lower material conc. (µg/ml). However, the cell survivability decreased significantly in BG than ZnBGs while the conc. increased from

2.5 to 50 µg/ml. Further, the assessment of normal NIH/3T3 cells incubated for 48h, 72h and 120h demonstrate significant decrease ($P<0.005$) in survivability in BG compared to ZnBGs despite being cultured in same material conc. Also the cell survivability over the scaffolds was decreased with prolongation of culture period even at the same material concentration. Interestingly, ZnBGs, especially Z2BG was found to be least toxic in NIH/3T3 as it might have caused minimal lysis than the other BGs. The 48h intra-group viability though significantly not different at higher conc. (10-50 µg/ml) but at lower conc. (2.5 and 5 µg/ml) the difference was statistically significant (at constant conc.). Likewise, the difference in viability was statistically significant ($P<0.005$) for Z2BG up to 25 µg/ml, and for Z3BG at 2.5 µg/ml. Moreover, the NIH/3T3 cells after 120h incubation into BGs exhibited significantly ($P<0.005$) higher cells in Z2BG and lowest in pure BG. The visual inspection of the live dead assay was also in accordance with the obvious rise in encapsulated cells in ZnBGs, particularly Z2BG.

The proliferation of the osteosarcoma cells incubated for 48h, 72h, and 120h demonstrate the significantly higher proliferated cells in ZnBGs, particularly in Z1BG. Unlike the previous cases, the dose (conc.) dependent proliferation study appeared higher in ZnBGs compared to BG but remained statistically insignificant in most observations. The only exception of Z1BG being the lowest in U2OS cellular proliferation was during 72h incubation at 50 µg/ml. Although insignificant, the BG was highest amongst the other BGs in U2OS cell populations for both 72h and 120h culture at 50 µg/ml. The confocal microscopic fluoresced images showing viable and apoptotic proliferated cells after 24h of culture over the scaffolds and subsequent staining with AO/PI was also found similar for the whole scaffold constructs. Still, it appeared a little more populated for Z2BG. The phase-contrast microscopic images

representing proliferation and viability of the BMSC, NIH/3T3, and U2OS cells were seemingly augmented in Z2BG, while the BG remained least compatible.

Further, the viability study using PBMC demonstrates similar compatibility for all of the BGs without any occurrence of comparable statistical difference. However, the *in vitro* effect of BMSCs upon glass scaffold implantation for 3days (Fig 4.10 A) and 10 days (Fig 4.10 B) observed by phase contrast and fluorescent microscopy showed the cells were more viable in Z2BG and Z3BG than the BG. Further, the 3d (Fig 4.10 A) and 10d (Fig 4.10 B) viability assay demonstrate retention of PI stain (red) within the dead or late apoptotic cells was more in BG than ZnBGs, which implies ZnBGs showed minimal cell lysis than BG.

The concentration-dependent cytotoxicity assay of U2OS, BMSC, NIH/3T3, and PBMC performed through LDH release demonstrates statistically insignificant cell lysis. However, the glass mediated cell (NIH/3T3) lysis was observed to be maximum but not always significant in BG except 2.5 and 5 µg/ml conc., while Z2BG was the least in lytic activity throughout the concentration-dependent cytotoxicity study. However, the lytic activity of the cells for different material conc. (i.e. 2 µg/ml vs. 50 µg/ml) was significantly ($P<0.005$) differed. Other than NIH/3T3, all other cells appeared to be highly, although insignificantly cytotoxic to Z2BG in most cases, particularly at higher dosage (i.e. 25 and 50 µg/ml). However, the cell lysis of U2OS, BMSC, and PBMC over the scaffold constructs was observed significantly higher only when the lysis of cells at higher conc. (i.e. 50 or 25 µg/ml) was compared with lysis in lower one (2.5 or 5 µg/ml).

### 4.5.3 Osteogenic ability of mBMSC upon BGs: alkaline phosphatase activity and osteogenic gene expression by RT-qPCR

The ubiquitous ALP, a homodimeric protein enzyme distributed throughout the biological organism from small bacteria (prokaryotes; E.Coli) to large mammalian (eukaryotes; plants,

animals) is accountable for multiple roles i.e. phosphate metabolism, liver and kidney function and calcification of bones(Sun et al., 2018, Sharma et al., 2014). ALP increases the phosphate concentration in alkaline environment by dephosphorylation of nonspecific pNPP substrate into pNP and inorganic phosphates through catalyzing the hydrolysis followed by $Ca^{2+}$ uptake, thereby enhances calcification in bone (Lai et al., 2015). Alkaline phosphatase is one of the key factors in commencement of mineralization through bone cell differentiation (Pauksch et al., 2014). The increase in ALP activity is associated with nucleation of bone minerals by coupling phosphates with calcium and their subsequent calcification (bone mineral formation), and thereby active bone formation (Ogata et al., 2005).In this investigation, a continuous increase in ALP activity with the increase in Zn percent in the scaffolds was observed. A multifold increase in ALP enzymatic activity for ZnBGs, particularly for Z3BG (about 17 times) against the BG (Fig 4.10 A) was observed. The increase in ALP activity for ZnBGs was due to the ability of the zinc in ZnBGs to induce osteogenic differentiation in BMSC (osteoprogenitor) to form osteoblast lineage (Hall et al., 1999, Cho et al., 2007, Ray et al., 2017). This findings suggest that ZnBGs accelerate osteogenic differentiation and promote early stage mineralization to form osteoblasts in comparison to BG. The upregulation of mid stage (after 10days) osteogenic marker OPN and later stage (after 21days) osteogenic marker OCN was also an indication of osteoblast differentiation (not shown after 10 days) (Ho et al., 2014, Lai et al., 2015). The significant upregulation ($P<0.005$) of the primer specific gene expression of the osteogenic genes (OPN and OCN) (Fig 4.10 C, D) in ZnBGs, particularly Z3BG, was due to the fact that zinc in ZnBG has induced the osteogenic potential of the BMSCs. The agarose gel electrophoretic images corresponding to band intensity of DNA fragments (Fig 4.10 B) were also clearly

supporting the higher intensity of ZnBGs in comparison with BG. However, the upregulation of OCN gene was not expressed as ALP (no gene expression shown) or OPN might be due to the natural inclination of the OCN genes to express at the later stage [after 21 days]. However, the upregulation of expression of these genes was anyway significantly higher for ZnBGs than BG, which is why zinc derived 1393 scaffolds (ZnBGs) are better osteogenic stimulator that supports better active bone forming ability than pure 1393 scaffold (BG).

### 4.5.4 Mechanical performances of BGs

The stress-strain curve (Fig 4.11) determines the fracture behavior as well as elasticity of the materials. The elasticity of materials is determined by the m (=tangent) value of the linear sections in stress-strain curves that pass through the origin. Herein, we have observed several peaks and valleys (zigzags) in the stress-strain curves which were most probably due to the buckling, crumbling, and collapsing of porous struts under mechanical load. However, the meandering in the curves were observed to be lessened as the metallic properties in the glasses were increased with increasing ZnO percent in the BG. The increase in mechanical properties for the ZnBGs could be due to several factors. Zn as a 'network modifier to intermediate element' could have altered the structural array of $SiO_4$ (Si-O-Si) tetrahedra to some extent by replacing Si (atomic radii 111 pm) to form Si-O-Zn in ZnBGs to enhance the inter-atomic compactness (Salman et al., 2017). Replacement of lighter atoms (Si) with heavier (Zn) ones also might have resulted in increased strengths. Therefore, the zinc addition reinforce the structure to enhance flexural properties and toughness (Ali et al., 2020). The observed strength is comparable to the highest compressive strength reported for the trabecular bone(Liu et al., 2013a, Liu et al., 2013b). Although the compressive and flexural strength has increased remarkably after ZnO

incorporation, yet these strengths are still not adequate to support the initial physiological load; and therefore need more advanced studies (like natural bone alike 1393 bioactive glass/polymer composite fabrication by 3D printing) to enhance the mechanical properties.

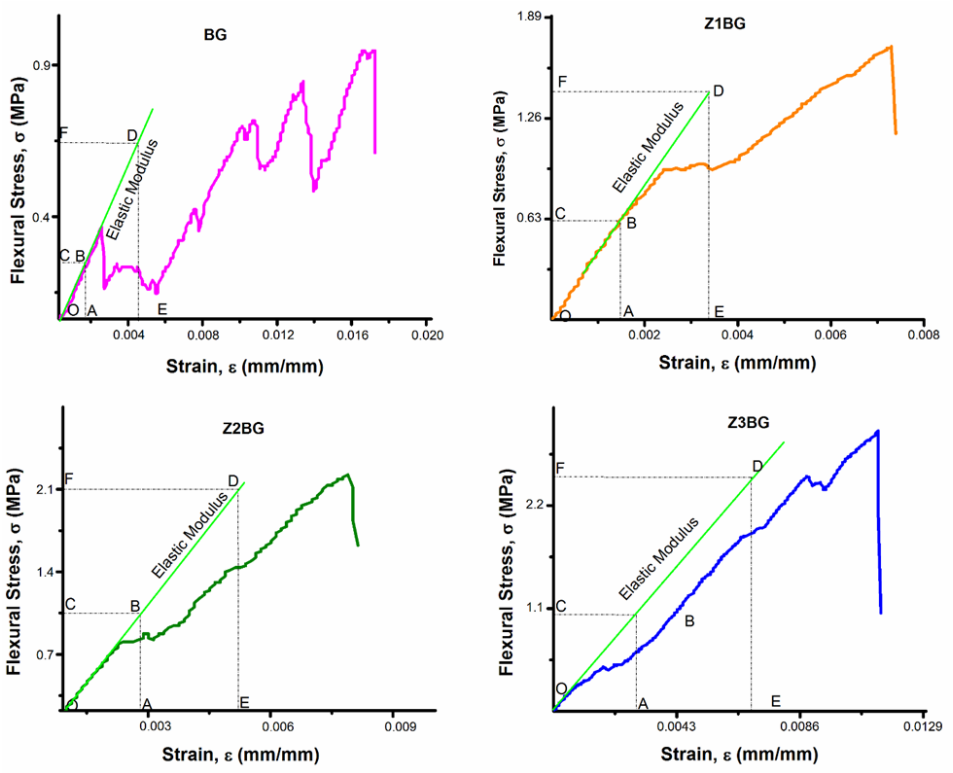


**Fig 4.11** Stress strain curves of BGs showing increasing Zn in BGs has increased in flexural modulus. The stress strain relationship in ZnBGs was appeared to have enhanced metallic nature as Zn in BGs was increased.

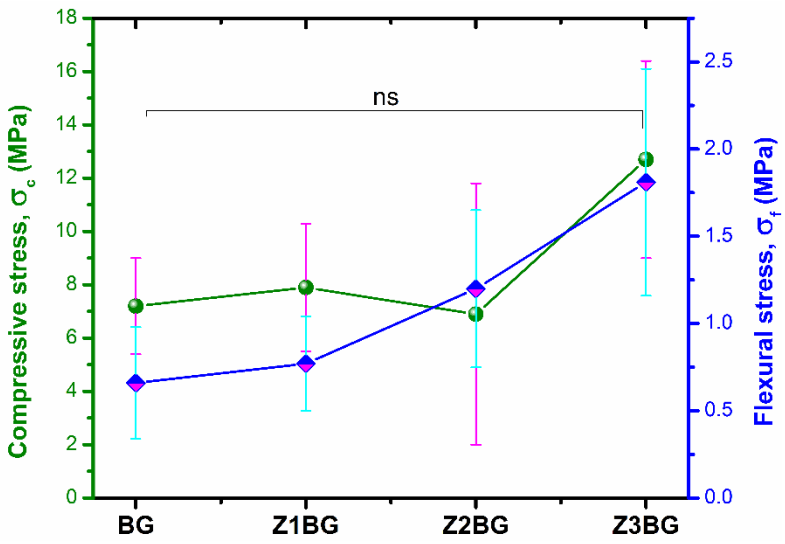


**Fig 4.12** Compressive strength and flexural strengths of the BG and ZnBGs. Compressive and flexural strengths were statistically analyzed for significant differences using One way ANOVA with tukey's post hoc mean comparison considering significant difference for the $p<0.05$; n=3.

## 4.6 Conclusions

In this study, we have successfully synthesized Zn derived glass based scaffolds mimicking trabecular bone with desired porosity and microstructure through sol gel route. Herein, we observed significant improvements in cytocompatibility in ZnBGs in comparison to BG. Moreover, the ALP activity and the primer specific osteogenic gene expression (OPN, OCN and GAPDH) indicate enhanced osteogenesis in ZnBGs. Also, the Zn incorporation has enhanced the mechanical performances of the ZNBGs. Therefore, ZnBGs can be considered as potential biomaterials for neo bone tissue regenerative application.